Spatially patterned spontaneous emission in a double-V-type quantum emitter near a plasmonic nanostructure

Hamid R. Hamedi [1,2,*], Viačeslav Kudriašov,[2,†] Seyyed Hossein Asadpour [3,‡] Julius Ruseckas [1,§]
Vassilios Yannopapas [4,‖] and Emmanuel Paspalakis [5,¶]

[1]*Baltic Institute of Advanced Technology, LT-01403 Vilnius, Lithuania*
[2]*Institute of Theoretical Physics and Astronomy, Vilnius University, LT-10257 Vilnius, Lithuania*
[3]*School of Physics, Institute for Research in Fundamental Sciences, IPM, Tehran 19395-5531, Iran*
[4]*Department of Physics, National Technical University of Athens, Athens 157 80, Greece*
[5]*Materials Science Department, School of Natural Sciences, University of Patras, Patras 265 04, Greece*

In this work, we propose a method to control spontaneous emission in a double-V-type quantum emitter near a plasmonic nanostructure using optical excitation with vortex beams. By leveraging the spatial and phase variations of the vortex beams, a spatially dependent interference and coherence of the upper energy states is induced, leading to an altered emission spectrum. The study reveals phenomena such as emission peak narrowing and merging, along with pattern conversion and redistribution in the transverse plane. Importantly, this method allows for remote distance control of spontaneous emission by tuning the separation between the quantum emitter and the plasmonic nanostructure, offering a new way to manipulate emission properties in hybrid quantum-plasmonic systems. This approach could find applications in quantum information processing and tunable nanoscale photonic devices.

I. INTRODUCTION

There are many fascinating phenomena happening when light interacts coherently with the quantum systems, among them electromagnetically induced transparency [1–3], coherent population trapping [4], lasing without inversion [5,6], and others [7–11]. Strong modification of the optical characteristics observed in these phenomena originates from the coherent control of the atomic states and quantum transitions in laser-driven media. The quantum interference (QI) plays a major role in many effects when alternative quantum pathways interfere in-phase (out-of-phase) leading to enhancement (suppression) of a specific transition, respectively [12–15]. Consequently, this can produce unusual optical conditions: cancellation of absorption or emission [16,17], or giant optical nonlinearities [11,18]. In recent decades these topics have garnered significant attention due to their importance for many prominent applications, including slow and stored light [19], precision optical sensing [10,20,21], and quantum information processing [22,23].

Coherent control of the spontaneous emission can be succeeded by QI between different spontaneous decay channels [24–31]. This topic has seen a widespread research employing various approaches and media types, aiming at better understanding of atom-photon interactions and creating advanced applications. One of the ways to regulate QI is by varying phase difference between the beams coherently exciting the upper states [26]. However, controlling spontaneous emission in most media is challenging due to the special requirements. QI relies on nonorthogonal electric dipoles of the spontaneous emission process, and can be maximized when the corresponding dipoles are almost parallel or antiparallel. Some researchers have simulated the required conditions by placing quantum emitters (QEs), like atoms, molecules, or semiconductor quantum dots, close to a photonic structure, which induces anisotropic Purcell effect [32]. This effect ideally suppresses the decay rate for one dipole orientation while maintaining it for the other. It was later suggested to place the QEs next to plasmonic nanostructures (PNs) to enhance QI, with its strength being controlled by adjusting the PN-QE separation [33–36]. This way, the control of light and matter interaction at the nanoscale becomes feasible. Different optical properties of hybrid plasmonic-quantum systems have been explored [34,37–42].

Many studies on coherent light-matter interaction in quantum systems have turned recently to the exploration of optical fields with more complex spatial profiles than the usual plane waves or Gaussian laser beams. Among those the beams with the orbital angular momentum (OAM) [43,44], commonly called optical vortices, should be emphasized. They have been extensively studied under different settings and for various optical media, demonstrating applications spanning optical communication [45], particle trapping [46,47], quantum information processing [48], quantum entanglement [49], and

---

*Contact author: hamid.hamedi@tfai.vu.lt
†Contact author: viaceslav.kudriasov@ff.vu.lt
‡Contact author: asadpour@ipm.ir
§Contact author: julius.ruseckas@gmail.com
‖Contact author: paspalak@upatras.gr
¶Contact author: vyannop@mail.ntua.gr

more [50–52]. Optical vortices, possessing additional degrees of freedom due to OAM, present advanced options to encode information and achieve more subtle control over the parameters of the optical medium. Previous investigations showed such phenomena as the OAM exchange between optical fields, control of light storage, and others. Moreover, due to the peculiar spatial and phase profile of the vortex beam (axial singularity and helical wavefront), it is possible to create specific spatial patterns and locally adjustable optical response of the atomic media [38,53,54]. Recently, the interaction of optical vortices with atoms in free-space has been used for the control of the spontaneous emission spectrum patterns emerging from the atoms [55,56].

In this paper we present an approach where the optical vortex beams are used to control the spatial distribution of the spontaneous emission in a coupled quantum-plasmonic medium. The system under study is a double-V-type QE containing four distinct energy levels. Two closely spaced upper states are excited from a single ground state with two laser beams, followed by the spontaneous decay from the excited levels to two lower states. This V-type atomic system is realized as a QE in the proximity of a PN which facilitates QI between the spontaneous-emission channels. Subsequently we introduce an approach for spontaneous-emission control by employing spatially inhomogeneous optical vortices as the pump fields, marking a significant departure from previous methods where control over QI was achieved solely through the variation of the relative phase between two laser fields [26,36]. In our case, there is a variable relative phase existing across the spatial profile of the pump beam. Such excitation leads to the inhomogeneous interaction and coherence between the excited states. Introducing spontaneous decay channels to this scheme forms a closed loop structure which exhibits a position-dependent spontaneous emission spectrum influenced by the vortex fields (similar to the spatially dependent EIT studied previously in [53]). Noteworthy observations arise, including the narrowing and merging of emission peaks, as well as the conversion and redistribution of patterns across the transverse plane. These phenomena are intricately guided by the relevant optical parameters, symmetries of excitation fields, and the distance between the QE and the PN.

II. THEORETICAL MODEL

We consider a model of QE with a double-V-type configuration consisting of two lower energy states $|0\rangle$, $|1\rangle$ and two upper energy states $|2\rangle$, $|3\rangle$, see Fig. 1(a). The system can be viewed as consisting of two linked V-type subsystems where upper energy levels form a closely spaced doublet. This system is excited by two laser fields with the equal optical frequencies and Rabi frequencies Ω_{02} and Ω_{03} coupling ground state $|0\rangle$ with the two upper states $|2\rangle$, $|3\rangle$. Both excited states $|2\rangle$, $|3\rangle$ decay spontaneously to the lower states $|0\rangle$, $|1\rangle$ with the corresponding decay rates γ_{21}, γ_{31} and γ'_{20}, γ'_{30}. For the closely spaced upper energy states we can assume that $\gamma_{21} = \gamma_{31} = \gamma$ and $\gamma'_{20} = \gamma'_{30} = \gamma'$. The QE located in vacuum at distance d from the surface of the PN consisting of a periodic array of metal-coated dielectric nanoparticles, which is shown in Figs. 1(b) and 1(c). Similarly to Ref. [36], we assume the decay to level $|1\rangle$ is facilitated by the surface plasmons of
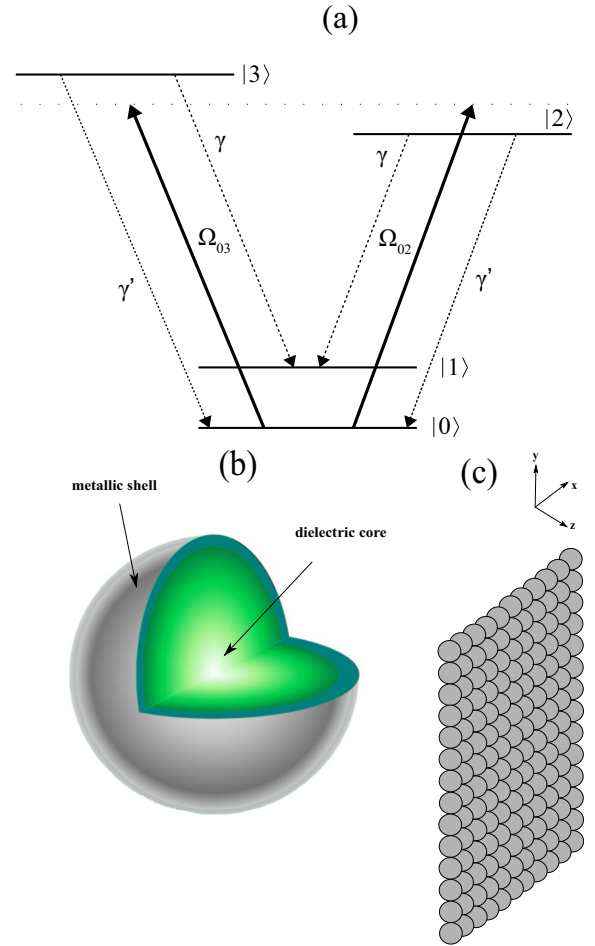

FIG. 1. (a) Energy level scheme of a double-V QE where two upper states decay spontaneously to two lower states after excitation by the pump fields. A metal-coated dielectric nanosphere (b) and a 2D array of such spheres (c).

the nearby PN, while the decay to $|0\rangle$ is only affected by the free-space vacuum modes.

In what follows we consider coupling fields Ω_{02} and Ω_{03} as optical vortices with the spatially dependent Rabi frequencies

$$\Omega_{02}(r, \phi) = |\Omega_{02}(r, \phi)|e^{il_2\phi} = |\Omega_{02}|\left(\frac{r}{w}\right)^{|l_2|} e^{-\frac{r^2}{w^2}} e^{il_2\phi}, \quad (1)$$

$$\Omega_{03}(r, \phi) = |\Omega_{03}(r, \phi)|e^{il_3\phi} = |\Omega_{03}|\left(\frac{r}{w}\right)^{|l_3|} e^{-\frac{r^2}{w^2}} e^{il_3\phi}, \quad (2)$$

where r and ϕ represent radial and azimuthal coordinates, respectively, and beam waist w is the same for both beams. Parameters l_2 and l_3 are the integer values corresponding to OAM numbers of the coupling beams. Note, that for some of our results we will take $l_3 = 0$, apparently in this case $\Omega_{03}(r, \phi)$ is reduced to a Gaussian beam with a plane wavefront.

The light-QE interaction in this setup (excluding spontaneous emission) can be described by the following Hamiltonian:

$$\hat{H} = \hbar\bar{\delta}_+|2\rangle\langle 2| + \hbar\bar{\delta}_-|3\rangle\langle 3| + \hbar\Omega_{02}(r, \phi)e^{i\delta t}|0\rangle\langle 2|$$
$$+ \hbar\Omega_{03}(r, \phi)e^{i\delta t}|0\rangle\langle 3| + \text{H.c.} \quad (3)$$

Following the wave function approach as in Ref. [36] and applying the Weisskopf-Wigner theory [26], the corresponding probability amplitudes c_2, c_3, $c_{\mathbf{k}}$ of both excited states and the emission mode obey the following system of differential equations

$$i\dot{c}_2(t) = \Omega_{20}c_0(t) + (\bar{\delta}_+ - i\bar{\gamma})c_2(t) - i\kappa c_3(t), \qquad (4)$$

$$i\dot{c}_3(t) = \Omega_{30}c_0(t) - i\kappa c_2(t) + (\bar{\delta}_- - i\bar{\gamma})c_3(t), \qquad (5)$$

$$i\dot{c}_{\mathbf{k}}(t) = \delta_{\mathbf{k}}c_{\mathbf{k}}(t) - ig_{\mathbf{k}2}c_2(t) - ig_{\mathbf{k}3}c_3(t). \qquad (6)$$

Here, $\bar{\delta}_\pm = \delta \pm \omega_{32}/2$ where $\delta = \omega - \bar{\omega}$ is the detuning of the applied field from the frequency $\bar{\omega} = (\omega_2 + \omega_3)/2 - \omega_0$, which represents the difference between the average energy of the upper states and that of the lower state; $\omega_{32} = \omega_3 - \omega_2$ is the energy difference between the upper states; $\bar{\gamma} = \gamma + \gamma'$ is the total spontaneous emission rate to both lower levels; $\Omega_{m0} = \Omega_{0m}^*(m = 2, 3)$ are the c.c. of the Rabi frequencies of the corresponding excitation transitions; $\mathbf{k}$ denotes the wave vector of the emitted photon; $g_{\mathbf{k}m}$ is the coupling constant of transition $|m\rangle \leftrightarrow |0\rangle$ with the $\mathbf{k}$th vacuum mode of frequency $\omega_{\mathbf{k}}$ and $\delta_{\mathbf{k}} = \omega_{\mathbf{k}} - \bar{\omega}$ denotes the frequency difference (see Ref. [36] for more details). The wave vector $\mathbf{k}$ indexes the so-called "vacuum modes," which in our case, refers to the photon states in the surrounding environment of the quantum system which is the lattice of plasmonic spheres. These modes are accounted for within the electromagnetic Green's tensor of the lattice of spheres.

The spontaneous emission rate γ and the coupling coefficient κ of the upper states can be expressed as $\gamma = (\Gamma_\perp + \Gamma_{||})/2$, $\kappa = (\Gamma_\perp - \Gamma_{||})/2$ [36]. Here, $\Gamma_\perp(\Gamma_{||})$ represent the normal (parallel) component of the spontaneous emission rate, respectively, which characterizes dipole orientation relative to the surface of the nanostructure. Mathematically, $\Gamma_\perp, \Gamma_{||}$ are expressed through the corresponding components of a dyadic electromagnetic Green's tensor as $\Gamma_{\perp,||} = \mu_0\mu^2\bar{\omega}^2\text{Im}(G_{\perp,||})/\hbar$ where $G_{\perp,||}(\mathbf{r}, \mathbf{r}; \bar{\omega})$ depends on the distance $\mathbf{r}$ of the QE from the surface of the PN and on the frequency $\bar{\omega}$. Using the above relations, the measure of QI can be introduced as $p = \kappa/\gamma = (\Gamma_\perp - \Gamma_{||})/(\Gamma_\perp + \Gamma_{||})$. The parameter p depends on the difference of the values of the decay rates $\Gamma_\perp$ and $\Gamma_{||}$ and can be nearly maximum ($|p| \approx 1$) when $\Gamma_\perp \gg \Gamma_{||}$ or $\Gamma_\perp \ll \Gamma_{||}$ and zero when $\Gamma_\perp = \Gamma_{||}$, where the latter is the condition in the vacuum. More details on the PN and also details on the calculation of the electromagnetic Green's tensor are presented in the Appendix.

The long-time spontaneous emission spectrum is given by $S(\delta_{\mathbf{k}}) \propto |c_{\mathbf{k}}(t \to \infty)|^2$, where

$$c_{\mathbf{k}}(t \to \infty) = \frac{-g_{\mathbf{k}2}K(\delta_{\mathbf{k}}) - g_{\mathbf{k}3}L(\delta_{\mathbf{k}})}{D(\delta_{\mathbf{k}})}. \qquad (7)$$

Thus,

$$S(\delta_{\mathbf{k}}) \propto \frac{|g_{\mathbf{k}2}|^2|K(\delta_{\mathbf{k}})|^2}{|D(\delta_{\mathbf{k}})|^2} + \frac{|g_{\mathbf{k}3}|^2|L(\delta_{\mathbf{k}})|^2}{|D(\delta_{\mathbf{k}})|^2}, \qquad (8)$$

where

$$K(\delta_{\mathbf{k}}) = ic_0(0)[\Omega_{20}\Delta_-(\delta_{\mathbf{k}}) - i\Omega_{30}\kappa] + ic_2(0)[\delta_{\mathbf{k}}\Delta_-(\delta_{\mathbf{k}}) - |\Omega_{03}|^2] - ic_3(0)[i\delta_{\mathbf{k}}\kappa - \Omega_{20}\Omega_{03}], \qquad (9)$$

$$L(\delta_{\mathbf{k}}) = ic_0(0)[\Omega_{30}\Delta_+(\delta_{\mathbf{k}}) - i\Omega_{20}\kappa] - ic_2(0)[i\delta_{\mathbf{k}}\kappa - \Omega_{02}\Omega_{30}] + ic_3(0)[\delta_{\mathbf{k}}\Delta_+(\delta_{\mathbf{k}}) - |\Omega_{02}|^2], \qquad (10)$$

$$D(\delta_{\mathbf{k}}) = \delta_{\mathbf{k}}[\Delta_+(\delta_{\mathbf{k}})\Delta_-(\delta_{\mathbf{k}}) + \kappa^2] - [|\Omega_{02}|^2\Delta_-(\delta_{\mathbf{k}}) + |\Omega_{03}|^2\Delta_+(\delta_{\mathbf{k}})] + i\kappa[\Omega_{20}\Omega_{03} + \Omega_{02}\Omega_{30}], \qquad (11)$$

and we used the notation for Δ_+ and Δ_- as

$$\Delta_\pm(\delta_{\mathbf{k}}) = \delta_{\mathbf{k}} - \bar{\delta}_\pm + i\bar{\gamma}. \qquad (12)$$

Note also that in the above expressions the Rabi frequencies Ω_{0m} and Ω_{m0} ($m = 2, 3$) represent the functions of the radial coordinates, i.e., $\Omega_{0m} = \Omega_{0m}(r, \phi)$ and $\Omega_{m0} = \Omega_{m0}(r, \phi)$.

III. SPONTANEOUS EMISSION IN DOUBLE-V-TYPE SYSTEM

In this section, we consider the spatial spontaneous emission distributions for various conditions of light-matter interaction in the double-V-type system. We investigate the dependence on several parameters, like the distance between QE and PN, different initial atomic states, and different OAM numbers of the coupling fields. We note that the two laser fields have a direction parallel to the PN so that they are not scattered off from it. Moreover, we can always make the waist w in Eqs. (1) and (2) such that is smaller than the distance between the QE and the NP. In any case, the results shown in Figs. 2–7 are in units of w, i.e., independent of the choice of

the waist of the incident beam. We will consider three scenarios with different PN-QE distances. Scenarios where the QE is in close proximity to the PN at a distance of $d = 0.1c/\omega_p$ are shown in the first two figures (Figs. 2 and 3). The situations where the QE is at an intermediate distance from the PN, with $d = 0.4c/\omega_p$, are shown in the subsequent two figures (Figs. 4 and 5). The cases where the QE is located at a long distance from the PN, specifically at $d = 0.9c/\omega_p$, are shown in the final two figures (Figs. 6 and 7). Figures 2, 4, and 6 correspond to scenarios where only the first beam possesses OAM $l_2 \neq 0$, while the other beam is nonvortex with $l_3 = 0$. Conversely, Figs. 3, 5, and 7 correspond to the cases where both beams exhibit OAM with opposite signs $l_2 = -l_3 \neq 0$. In addition, panel (a) of each figure shows the scenario where the QE is in its ground state, with $c_0 = 1$, $c_2 = c_3 = 0$, while panel (b) showcases QE in an equal superposition of the excited states $c_0 = 0$, $c_2 = c_3 = 1/\sqrt{2}$.

In what follows we will consider a situation where energy splitting between upper energy levels is zero. In this case $\delta_{\mathbf{k}} = \delta = \omega_{32} = 0$ and $\bar{\delta}_\pm = 0$. Also, the decay rates are considered to be equal $\gamma' = \gamma'_{20} = \gamma'_{30} = \Gamma_0$, where Γ_0 is the decay rate
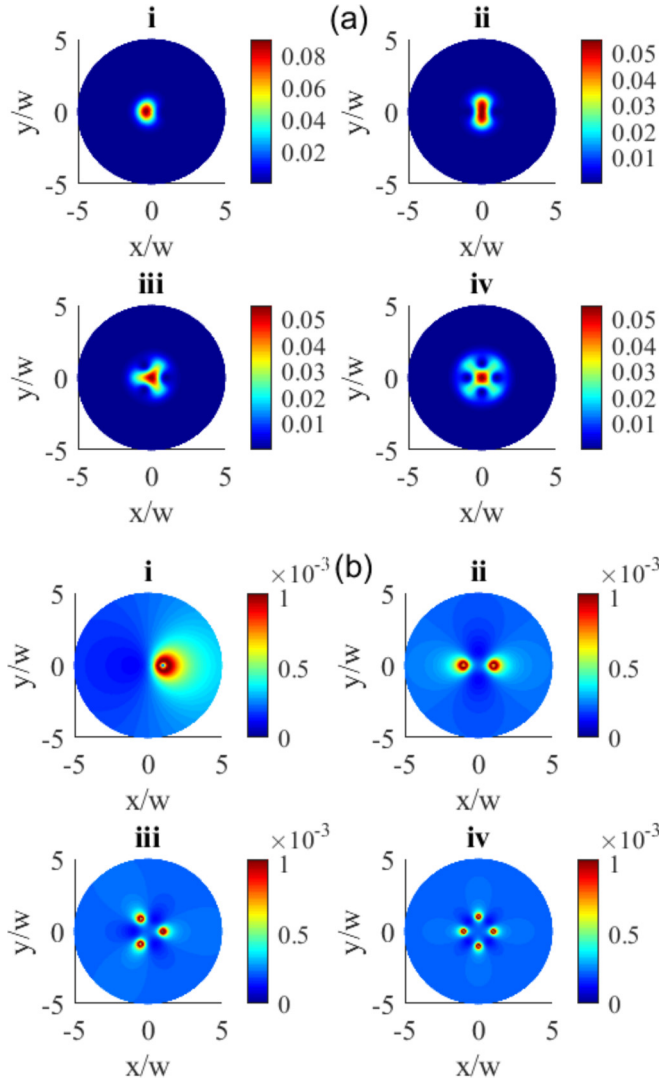
FIG. 2. Transverse patterns of the spontaneous emission $S(\delta_\mathbf{k})/S(0)$. Here $d = 0.1c/\omega_p$. Initial state: (a) $c_0 = 1, c_2 = c_3 = 0$, (b) $c_0 = 0, c_2 = c_3 = 1/\sqrt{2}$. OAM numbers: (i) $l_2 = 1$, (ii) $l_2 = 2$, (iii) $l_2 = 3$, (iv) $l_2 = 4$ and $l_3 = 0$.

FIG. 3. Transverse patterns of the spontaneous emission $S(\delta_\mathbf{k})/S(0)$. Here $d = 0.1c/\omega_p$. Initial state: (a) $c_0 = 1, c_2 = c_3 = 0$, (b) $c_0 = 0, c_2 = c_3 = 1/\sqrt{2}$. OAM numbers: (i) $l_2 = -l_3 = 1$, (ii) $l_2 = -l_3 = 2$, (iii) $l_2 = -l_3 = 3$, (iv) $l_2 = -l_3 = 4$.

of the upper states $|2\rangle$ and $|3\rangle$ to the lower state $|1\rangle$ in the vacuum. Values of γ and κ vary with the distance d to the PN, since the parameters $\Gamma_\perp$ and $\Gamma_\parallel$ are distance dependent. The coupling fields are assumed having the same amplitudes $|\Omega_{02}| = |\Omega_{03}| = \Gamma_0$.

Taking into consideration the above conditions, we have $\Delta_+ = \Delta_- = i\bar{\gamma}$, so the previous relations for K, L, D reduce to

$$K = -c_0(0)[\Omega_{20}\bar{\gamma} - \Omega_{30}\kappa] - ic_2(0)|\Omega_{03}|^2 + ic_3(0)\Omega_{20}\Omega_{03}, \tag{13}$$

$$L = -c_0(0)[\Omega_{30}\bar{\gamma} - \Omega_{20}\kappa] + ic_2(0)\Omega_{02}\Omega_{30} - ic_3(0)|\Omega_{02}|^2, \tag{14}$$

$$D = -i\bar{\gamma}[|\Omega_{02}|^2 + |\Omega_{03}|^2] + i\kappa[\Omega_{20}\Omega_{03} + \Omega_{02}\Omega_{30}]. \tag{15}$$

Depending on the initial state of QE, these quantities can be further reduced. For example, in the case of $c_0 = 1$,

$c_2 = c_3 = 0$ the QE is in the ground state and K and L take the following form:

$$K = \Omega_{30}(r, \phi)\kappa - \Omega_{20}(r, \phi)\bar{\gamma}, \tag{16}$$

$$L = \Omega_{20}(r, \phi)\kappa - \Omega_{30}(r, \phi)\bar{\gamma}. \tag{17}$$

On the other hand, in the case of $c_0 = 0, c_2 = c_3 = 1/\sqrt{2}$ the QE is in the excited superposition state with

$$K = \frac{i}{\sqrt{2}}[\Omega_{20}(r, \phi)\Omega_{03}(r, \phi) - |\Omega_{03}(r, \phi)|^2], \tag{18}$$

$$L = \frac{i}{\sqrt{2}}[\Omega_{02}(r, \phi)\Omega_{30}(r, \phi) - |\Omega_{02}(r, \phi)|^2]. \tag{19}$$

Here we explicitly put the dependencies of the corresponding Rabi frequencies on the radial coordinates.
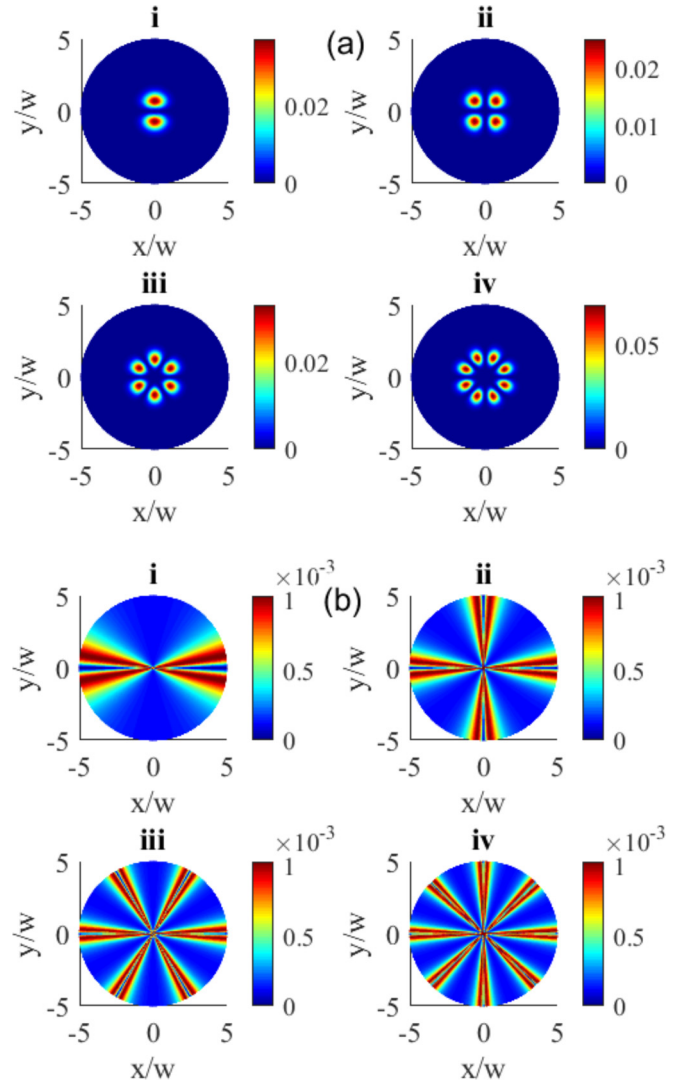
FIG. 4. Transverse patterns of the spontaneous emission $S(\delta_{\mathbf{k}})/S(0)$. Here $d = 0.4c/\omega_p$. Initial state: (a) $c_0 = 1, c_2 = c_3 = 0$, (b) $c_0 = 0, c_2 = c_3 = 1/\sqrt{2}$. OAM numbers: (i) $l_2 = 1$, (ii) $l_2 = 2$, (iii) $l_2 = 3$, (iv) $l_2 = 4$ and $l_3 = 0$.
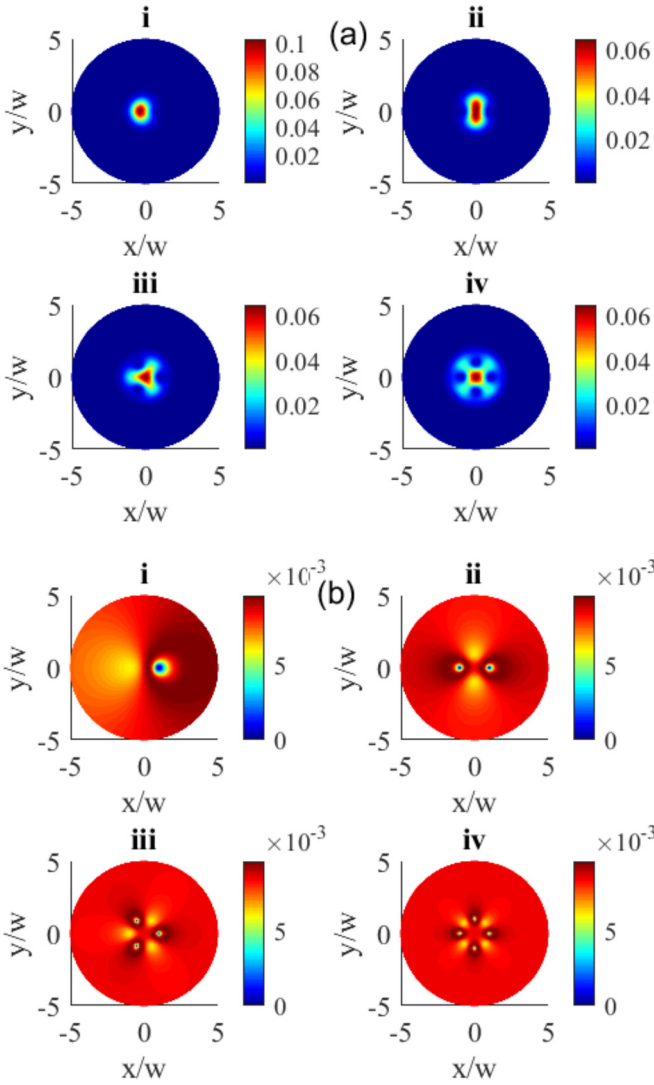

FIG. 5. Transverse patterns of the spontaneous emission $S(\delta_{\mathbf{k}})/S(0)$. Here $d = 0.4c/\omega_p$. Initial state: (a) $c_0 = 1, c_2 = c_3 = 0$, (b) $c_0 = 0, c_2 = c_3 = 1/\sqrt{2}$. OAM numbers: (i) $l_2 = -l_3 = 1$, (ii) $l_2 = -l_3 = 2$, (iii) $l_2 = -l_3 = 3$, (iv) $l_2 = -l_3 = 4$.

A. QE at close distance

We start our analysis for the case where QE is located at a short distance to the PN with $d = 0.1c/\omega_p$. In the case of a vortex and a Gaussian beam used as excitation fields (Fig. 2), one can see that both plots show the signature of the OAM symmetry in the spontaneous emission spectra. This is indicated by the shape of the emission structures in the middle part of the beam, having azimuthal symmetry corresponding to the OAM number $l_2 = 1, 2, 3, 4$ of only one vortex beam. This symmetry matches the symmetry of the interference pattern between optical vortex and a plane wave, which is eventually imprinted onto the spontaneous emission. However, the quality of the patterns are different for the cases when the QE is in the ground state [Fig. 2(a)] or in the superposition of states [Fig. 2(b)]. One can see that the emission peaks on panel (a) do not coincide with the peaks on panel (b), also the emission structures are rotated by some small angle (45°) with respect to both cases. As indicated on the scale, the
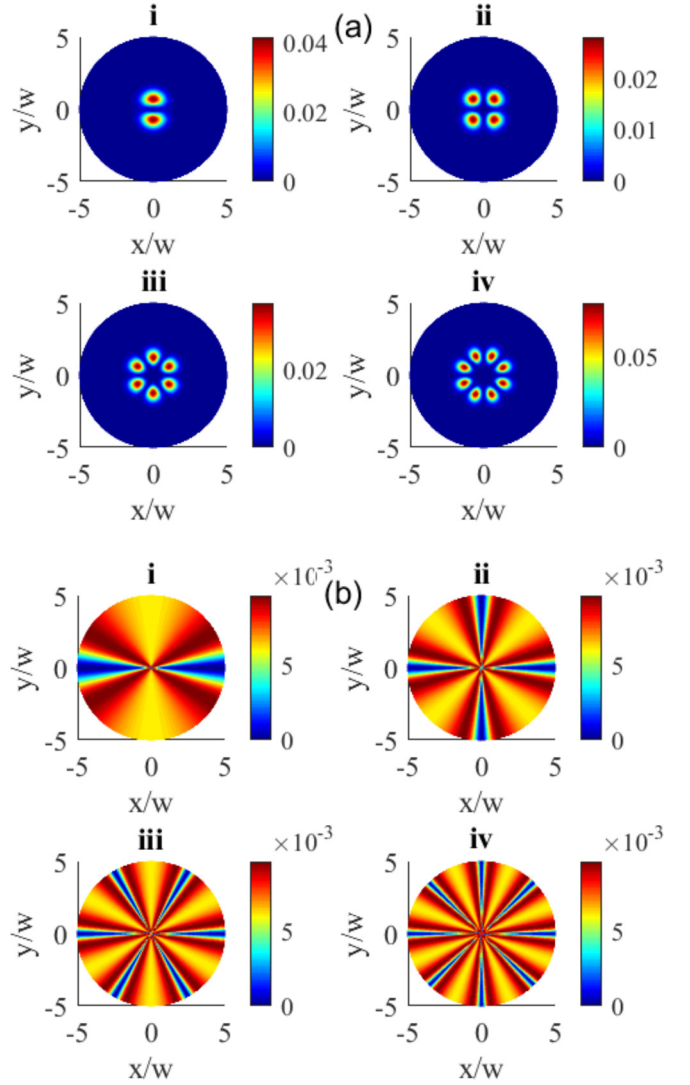
general level of spontaneous emission is lower on [Fig. 2(b)] compared to the plot [Fig. 2(a)]. Moreover, in Fig. 2(b) we can observe much highly developed and narrower emission peaks which get even more pronounced with the increased OAM number.

In the case of two vortex beams with the opposite vortices (Fig. 3), there is a change in the pattern symmetry. One can see that for the both plots the azimuthal symmetry angle is reduced by two, in accordance with the symmetry pattern between two vortex beams having equal and opposite OAM numbers: $l_2 + l_3 = 2l_2 = 2, 4, 6, 8$. Notably, the emission at the central part of the distribution is absent for the case of two vortex beams when the QE initially in the ground state [Fig. 3(a)]. Here, the emission peaks are also a lot more pronounced if compared to the previous case with only one vortex beam [Fig. 2(a)]. Moreover, in contrast to the previous plots in Fig. 2(b), those shown in Fig. 3(b) show completely different spatial structure. Here, the emission patterns do not exhibit
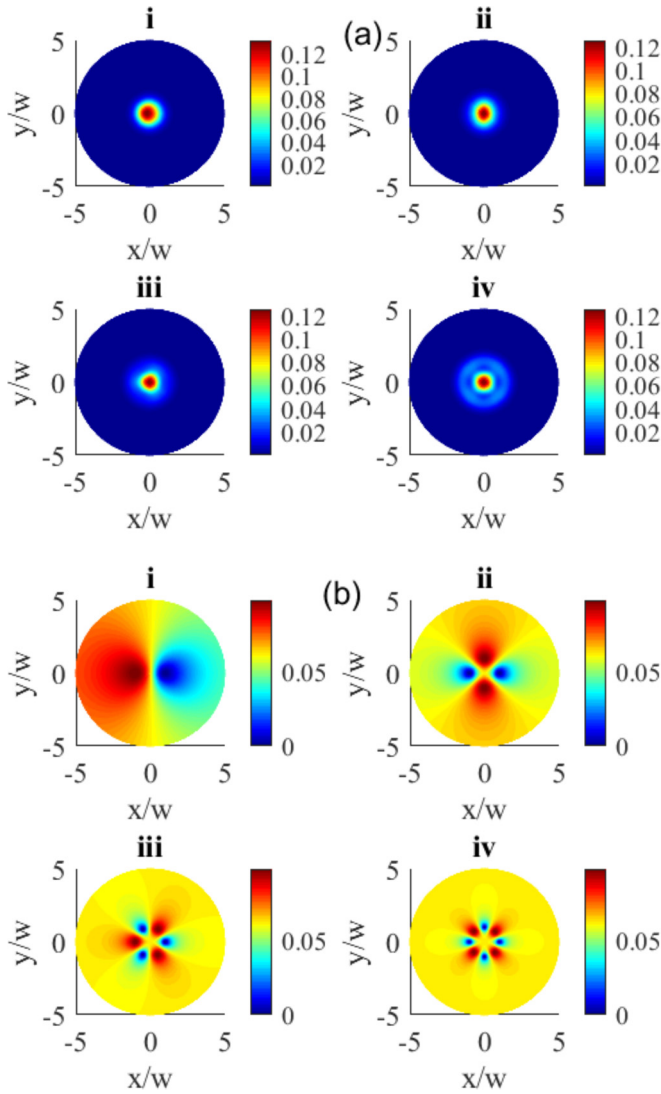
FIG. 6. Transverse patterns of the spontaneous emission $S(\delta_{\mathbf{k}})/S(0)$. Here $d = 0.9c/\omega_p$. Initial state: (a) $c_0 = 1$, $c_2 = c_3 = 0$, (b) $c_0 = 0$, $c_2 = c_3 = 1/\sqrt{2}$. OAM numbers: (i) $l_2 = 1$, (ii) $l_2 = 2$, (iii) $l_2 = 3$, (iv) $l_2 = 4$ and $l_3 = 0$.

FIG. 7. Transverse patterns of the spontaneous emission $S(\delta_{\mathbf{k}})/S(0)$. Here $d = 0.9c/\omega_p$. Initial state: (a) $c_0 = 1$, $c_2 = c_3 = 0$, (b) $c_0 = 0$, $c_2 = c_3 = 1/\sqrt{2}$. OAM numbers: (i) $l_2 = -l_3 = 1$, (ii) $l_2 = -l_3 = 2$, (iii) $l_2 = -l_3 = 3$, (iv) $l_2 = -l_3 = 4$.

any localized peaks, instead, there are extended directions in the transverse plane along which the emission preferably happens. The angular location of these directions do not coincide with the angular positions of emission peaks in Fig. 3(a). One can also notice that the emission areas broaden with increase of a radial distance.

B. QE at intermediate distance

Next we analyze the situation of QE located at the intermediate distance $d = 0.4c/\omega_p$ to the PN. For a vortex beam and plane wave the emission plots are quite similar qualitatively and quantitatively to those for the closely located QE when the QE is initially in the ground state [Fig. 4(a)]. On the contrary, when the QE is initially prepared in a superposition of the upper states [Fig. 4(b)], the patterns undergo significant changes. This primarily manifests as a much higher background emission compared to the emission peak heights. Qualitatively, the
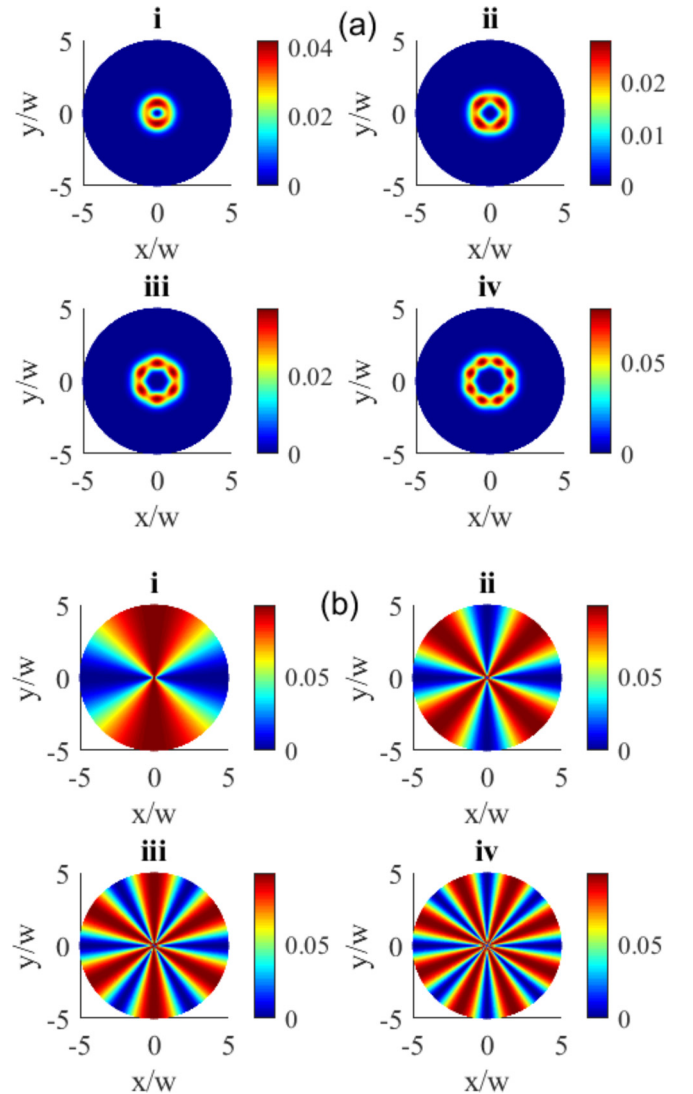
structure is similar to that for a closely located QE [Fig. 2(b)], but the overall background level is more pronounced here. Moreover, the sources of underdeveloped secondary emission peaks can be noticed in Fig. 4(b) which are located between the main ones. Both main and secondary peaks share the same azimuthal symmetry corresponding to l_2, but are rotated by 45° with respect to each other.

For the vortex beams with opposite vorticities (Fig. 5), the patterns resemble those for the closely located QE. On the other hand, for the case in Fig. 5(b), much more pronounced background and higher levels of spontaneous emission is observable, with the directional emission features appearing more broad and extended compared to Fig. 3(b).

C. QE at long distance

Finally, we consider the situation with distantly located QE when $d = 0.9c/\omega_p$. For this situation the spatial distributions

become quite distinct from those previously discussed. For the vortex beam and plane wave case for QE initiated in the ground state [Fig. 6(a)] the emission structures become more spread and look somewhat merged, or even structureless, exhibiting a single broad peak at the center. Because of that, the underlying symmetry is harder to distinguish here, although it is still present. On the contrary, for the case of superposition state [Fig. 6(b)], a lot more variations happen compared to the previous plots. The overall background level is reduced, while the emission peaks seen in the previous plots turn into emission minima. Moreover, secondary minimas become strongly pronounced. Both major and minor minima peaks exhibit the same symmetry each, as previously, rotated by $45°$ angle with respect to each other.

For the vortex beams with opposite vorticities with the initial condition $c_0 = 1$, $c_2 = c_3 = 0$ [Fig. 7(a)], the distinct peak pattern becomes merged while retaining no emission at the beam central part. Plot for initial condition $c_0 = 0$, $c_2 = c_3 = 1/\sqrt{2}$ [Fig. 7(b)] shows a high contrast structure with the pronounced directional features along which emission is observed. The emission shape broadens with the increase of the radial distance.

IV. SUMMARY

In summary, we proposed a method to achieve the control over spontaneous emission in double-V-type shape QE in the vicinity of a PN, using optical excitation with vortex beams. Specifically, the inhomogeneous spatial and phase profile of the excitation by vortex beams allows to induce spatially variable phase difference in the transverse plane, leading to spatially dependent interference and variable coherence of the upper energy states. Consequently, it results in spatially dependent spontaneous emission spectrum, which has been analyzed depending on different laser-matter interaction parameters, such as the QE distance from the PN, the initial state of the QE, and the vorticities of the excitation optical beams. Our research revealed interesting findings, like emission peak narrowing and merging, pattern conversion and redistribution across the transverse plane guided both by the aforementioned parameters and the underlying symmetries of the excitation fields. This approach can be used further in theoretical investigations or in the applied tasks to obtain spatial control of the spontaneous emission. The proposed method could allow for the control of optical chirality [57] of the emitted light by employing chiral plasmonic nanostructures.

ACKNOWLEDGMENT

APPENDIX: CALCULATION OF THE SPONTANEOUS EMISSION RATES NEAR A PLASMONIC NANOSTRUCTURE

The focus of the current study is a PN consisting of a 2D square lattice of silica nanospheres coated with metal [see Figs. 1(b) and 1(c)]. The periodic arrangement of these nanospheres can be achieved through various techniques, such as self-assembly [58], nanopatterning, and nanolithography [59]. The presence of a small/moderate disorder is not expected to significantly impact our results as we operate in the long-wavelength limit and the influence of disorder is a widening of the plasmonic peaks [60]. The dielectric function of the metal-coated nanoshell is described by a Drude-type electric permittivity [33,35]

$$\epsilon(\omega) = 1 - \frac{\omega_p^2}{\omega(\omega + i/\tau)}, \tag{A1}$$

where ω_p and τ are the bulk plasma frequency and the relaxation time of the conduction-band electrons of the metal, respectively. A typical value of the plasma frequency for gold is $\hbar\omega_p = 8.99\,\text{eV}$. This also determines the length scale of the system as $c/\omega_p \approx 22\,\text{nm}$. The dielectric constant of SiO$_2$ is taken to be $\epsilon = 2.1$. In the calculations we have taken $\tau^{-1} = 0.05\omega_p$. The lattice constant of the square lattice is $a = 2c/\omega_p$ and the sphere radius $S = c/\omega_p$ with the core radius $S_c = 0.7c/\omega_p$.

The electromagnetic Green's tensor, which provides the relevant spontaneous emission rates $\Gamma_\perp$ and $\Gamma_\parallel$, is described by [61,62]

$$G_{ii'}^{EE}(\mathbf{r}, \mathbf{r}; \bar{\omega}) = g_{ii'}^{EE}(\mathbf{r}, \mathbf{r}; \omega) - \frac{i}{8\pi^2} \iint_{\text{SBZ}} d^2\mathbf{k}_\parallel \sum_{\mathbf{g}} \frac{1}{c^2 K_{\mathbf{g};z}^+}$$
$$\times v_{\mathbf{g}\mathbf{k}_\parallel;i}(\mathbf{r}) \exp(-i\mathbf{K}_{\mathbf{g}}^+ \cdot \mathbf{r})\hat{\mathbf{e}}_{i'}(\mathbf{K}_{\mathbf{g}}^+), \tag{A2}$$

where the function $v_{\mathbf{g}\mathbf{k}_\parallel;i}(\mathbf{r})$ is defined as

$$v_{\mathbf{g}\mathbf{k}_\parallel;i}(\mathbf{r}) = \sum_{\mathbf{g}'} R_{\mathbf{g}';\mathbf{g}}(\omega, \mathbf{k}_\parallel) \exp(-i\mathbf{K}_{\mathbf{g}'}^- \cdot \mathbf{r})\hat{\mathbf{e}}_i(\mathbf{K}_{\mathbf{g}'}^-). \tag{A3}$$

The vectors $\mathbf{g}$ represent the reciprocal-lattice vectors associated with the 2D periodic arrangement of the scatterer plane. Concurrently, $\mathbf{k}_\parallel$ correspond to the reduced wave vector residing within the surface Brillouin zone of the reciprocal lattice formed by the spheres [63]. The vector $\mathbf{K}_{\mathbf{g}}^\pm$ is given by

$$\mathbf{K}_{\mathbf{g}}^\pm = \{\mathbf{k}_\parallel + \mathbf{g} \pm [q^2 - (\mathbf{k}_\parallel + \mathbf{g})^2]^{1/2}\}. \tag{A4}$$

When $q^2 = \omega^2/c^2 < (k_\parallel + \mathbf{g})^2$, the wave vector $\mathbf{K}_{\mathbf{g}}^\pm$ takes on an imaginary component, resulting in the formation of an evanescent wave. In Eq. (A2), the term $g_{ii'}^{EE}(\mathbf{r}, \mathbf{r}; \omega)$ represents the Green's tensor in free space, while $\hat{\mathbf{e}}_i(\mathbf{K}_{\mathbf{g}}^\pm)$ denotes the normalized polarization vector orthogonal to $\mathbf{K}_{\mathbf{g}}^\pm$. In addition, the reflection matrix $R_{\mathbf{g}';\mathbf{g}}(\omega, \mathbf{k}_\parallel)$ combines the contributions of reflected (diffracted) beams resulting from the incidence of a plane wave from the left side of the scatterer plane, incorporating all $\mathbf{g}'$. It is worth noting that components related to s-polarized waves, which involve the unit vector $\hat{\mathbf{e}}_i(\mathbf{K}_{\mathbf{g}}^\pm)$ perpendicular to $\mathbf{K}_{\mathbf{g}}^\pm$, have a negligible impact on the overall decay rates. Consequently, they are intentionally disregarded in Eq. (A2) [63].

[1] M. Fleischhauer, A. Imamoglu, and J. P. Marangos, Electromagnetically induced transparency: Optics in coherent media, Rev. Mod. Phys. **77**, 633 (2005).

[2] K.-J. Boller, A. Imamoğlu, and S. E. Harris, Observation of electromagnetically induced transparency, Phys. Rev. Lett. **66**, 2593 (1991).

[3] E. Paspalakis and P. L. Knight, Electromagnetically induced transparency and controlled group velocity in a multilevel system, Phys. Rev. A **66**, 015802 (2002).

[4] B. J. Dalton and P. L. Knight, The effects of laser field fluctuations on coherent population trapping, J. Phys. B: At. Mol. Phys. **15**, 3997 (1982).

[5] Y. Zhu, Lasing without inversion in a closed three-level system, Phys. Rev. A **45**, R6149 (1992).

[6] J. Mompart and R. Corbalan, Lasing without inversion, J. Opt. B: Quantum Semiclass. Opt. **2**, R7 (2000).

[7] Y. Wu and L. Deng, Ultraslow optical solitons in a cold four-state medium, Phys. Rev. Lett. **93**, 143904 (2004).

[8] Y. Wu and L. Deng, Ultraslow bright and dark optical solitons in a cold three-state medium, Opt. Lett. **29**, 2064 (2004).

[9] J. Ruseckas, V. Kudriašov, G. Juzeliūnas, R. G. Unanyan, J. Otterbach, and M. Fleischhauer, Photonic-band-gap properties for two-component slow light, Phys. Rev. A **83**, 063811 (2011).

[10] E. Paspalakis and P. L. Knight, Localizing an atom via quantum interference, Phys. Rev. A **63**, 065802 (2001).

[11] H. R. Hamedi and G. Juzeliūnas, Phase-sensitive kerr nonlinearity for closed-loop quantum systems, Phys. Rev. A **91**, 053823 (2015).

[12] P. Zhou and S. Swain, Quantum interference in resonance fluorescence for a driven V atom, Phys. Rev. A **56**, 3011 (1997).

[13] Z. Ficek and T. Rudolph, Quantum interference in a driven two-level atom, Phys. Rev. A **60**, R4245 (1999).

[14] H. Huang, S.-Y. Zhu, and M. S. Zubairy, Nondecaying state in a three-level system driven by a single field: Effect of relaxations, Phys. Rev. A **55**, 744 (1997).

[15] N. P. Georgiades, E. S. Polzik, and H. J. Kimble, Quantum interference in two-photon excitation with squeezed and coherent fields, Phys. Rev. A **59**, 676 (1999).

[16] K. Yamamoto, K. Ichimura, and N. Gemma, Enhanced and reduced absorptions via quantum interference: Solid system driven by a rf field, Phys. Rev. A **58**, 2460 (1998).

[17] Z. Ficek and S. Swain, Quantum interference in optical fields and atomic radiation, J. Mod. Opt. **49**, 3 (2002).

[18] Y. Niu and S. Gong, Enhancing kerr nonlinearity via spontaneously generated coherence, Phys. Rev. A **73**, 053811 (2006).

[19] X. Wang, J. Wang, Z. Ren, R. Wen, C.-L. Zou, G. A. Siviloglou, and J. F. Chen, Quantum interference between photons and single quanta of stored atomic coherence, Phys. Rev. Lett. **128**, 083605 (2022).

[20] G. S. Agarwal and K. T. Kapale, Subwavelength atom localization via coherent population trapping, J. Phys. B: At. Mol. Opt. Phys. **39**, 3437 (2006).

[21] J. A. Miles, Z. J. Simmons, and D. D. Yavuz, Subwavelength localization of atomic excitation using electromagnetically induced transparency, Phys. Rev. X **3**, 031014 (2013).

[22] M. Stobińska, A. Buraczewski, M. Moore, W. R. Clements, J. J. Renema, S. W. Nam, T. Gerrits, A. Lita, W. S. Kolthammer, A. Eckstein, and I. A. Walmsley, Quantum interference enables constant-time quantum information processing, Sci. Adv. **5**, eaau9674 (2019).

[23] K. R. Patton and U. R. Fischer, Hybrid of superconducting quantum interference device and atomic Bose-Einstein condensate: An architecture for quantum information processing, Phys. Rev. A **87**, 052303 (2013).

[24] S.-Y. Zhu and M. O. Scully, Spectral line elimination and spontaneous emission cancellation via quantum interference, Phys. Rev. Lett. **76**, 388 (1996).

[25] F. Ghafoor, S.-Y. Zhu, and M. S. Zubairy, Amplitude and phase control of spontaneous emission, Phys. Rev. A **62**, 013811 (2000).

[26] E. Paspalakis and P. L. Knight, Phase control of spontaneous emission, Phys. Rev. Lett. **81**, 293 (1998).

[27] J.-H. Wu, A.-J. Li, Y. Ding, Y.-C. Zhao, and J.-Y. Gao, Control of spontaneous emission from a coherently driven four-level atom, Phys. Rev. A **72**, 023802 (2005).

[28] L. Jia-Hua, L. Ji-Bing, C. Ai-Xi, and Q. Chun-Chao, Spontaneous emission spectra and simulating multiple spontaneous generation coherence in a five-level atomic medium, Phys. Rev. A **74**, 033816 (2006).

[29] R. Arun, Interference-induced splitting of resonances in spontaneous emission, Phys. Rev. A **77**, 033820 (2008).

[30] A.-J. Li, X.-L. Song, X.-G. Wei, L. Wang, and J.-Y. Gao, Effects of spontaneously generated coherence in a microwave-driven four-level atomic system, Phys. Rev. A **77**, 053806 (2008).

[31] C. L. Wang, Z. H. Kang, S. C. Tian, and J. H. Wu, Control of spontaneous emission from a microwave driven atomic system, Opt. Express **20**, 3509 (2012).

[32] G. S. Agarwal, Anisotropic vacuum-induced interference in decay channels, Phys. Rev. Lett. **84**, 5500 (2000).

[33] S. Evangelou, V. Yannopapas, and E. Paspalakis, Transparency and slow light in a four-level quantum system near a plasmonic nanostructure, Phys. Rev. A **86**, 053811 (2012).

[34] H. R. Hamedi, V. Yannopapas, G. Juzeliūnas, and E. Paspalakis, Coherent optical effects in a three-level quantum emitter near a periodic plasmonic nanostructure, Phys. Rev. B **106**, 035419 (2022).

[35] F. Carreño, M. A. Antón, V. Yannopapas, and E. Paspalakis, Control of the absorption of a four-level quantum system near a plasmonic nanostructure, Phys. Rev. B **95**, 195410 (2017).

[36] S. Evangelou, V. Yannopapas, and E. Paspalakis, Modifying free-space spontaneous emission near a plasmonic nanostructure, Phys. Rev. A **83**, 023819 (2011).

[37] H. R. Hamedi, V. Yannopapas, and E. Paspalakis, Spatially structured optical effects in a four-level quantum system near a plasmonic nanostructure, Ann. Phys. (Berlin) **533**, 2100117 (2021).

[38] H. R. Hamedi, V. Yannopapas, E. Paspalakis, and J. Ruseckas, Spatially patterned light amplification without inversion, Results Phys. **54**, 107135 (2023).

[39] H. Chen, J. Ren, Y. Gu, D. Zhao, J. Zhang, and Q. Gong, Nanoscale kerr nonlinearity enhancement using spontaneously generated coherence in plasmonic nanocavity, Sci. Rep. **5**, 18315 (2016).

[40] J. Ren, H. Chen, Y. Gu, D. Zhao, H. Zhou, J. Zhang, and Q. Gong, Plasmon-enhanced kerr nonlinearity via subwavelength-confined anisotropic purcell factors, Nanotechnology **27**, 425205 (2016).

[41] S. H. Asadpour and H. R. Soleimani, Phase dependence of optical bistability and multistability in a four-level quantum

system near a plasmonic nanostructure, J. Appl. Phys. **119**, 023102 (2016).

[42] M. Klein, R. Binder, M. R. Koehler, D. G. Mandrus, T. Taniguchi, K. Watanabe, and J. R. Schaibley, Slow light in a 2D semiconductor plasmonic structure, Nat. Commun. **13**, 6216 (2022).

[43] L. Allen, M. W. Beijersbergen, R. J. C. Spreeuw, and J. P. Woerdman, Orbital angular momentum of light and the transformation of Laguerre-Gaussian laser modes, Phys. Rev. A **45**, 8185 (1992).

[44] A. M. Yao and M. J. Padgett, Orbital angular momentum: Origins, behavior and applications, Adv. Opt. Photonics **3**, 161 (2011).

[45] S. Suciu, G. A. Bulzan, T.-A. Isdrailă, A. M. Pălici, S. Ataman, C. Kusko, and R. Ionicioiu, Quantum communication networks with optical vortices, Phys. Rev. A **108**, 052612 (2023).

[46] M. P. Macdonald, L. Paterson, K. V. Sepulveda, J. Arlt, W. Sibbett, and K. Dholakia, Creation and manipulation of three-dimensional optically trapped structures, Science **296**, 1101 (2002).

[47] M. Woerdemann, C. Alpmann, M. Esseling, and C. Denz, Advanced optical trapping by complex beam shaping, Laser Photon. Rev. **7**, 839 (2013).

[48] J. Wang, F. Castellucci, and S. Franke-Arnold, Vectorial light–matter interaction: Exploring spatially structured complexlight fields, AVS Quantum Sci. **2**, 031702 (2020).

[49] A. Mair, A. Vaziri, G. Weihs, and A. Zeilinger, Entanglement of the orbital angular momentum states of photons, Nature (London) **412**, 313 (2001).

[50] F. Tamburini, B. Thidé, I. Licata, F. Bouchard, and E. Karimi, Majorana bosonic quasiparticles from twisted photons in free space, Phys. Rev. A **103**, 033505 (2021).

[51] A. Sit, R. Fickler, F. Alsaiari, F. Bouchard, H. Larocque, P. Gregg, L. Yan, R. W. Boyd, S. Ramachandran, and E. Karimi, Quantum cryptography with structured photons through a vortex fiber, Opt. Lett. **43**, 4108 (2018).

[52] F. Castellucci, T. W. Clark, A. Selyem, J. Wang, and S. Franke-Arnold, Atomic compass: Detecting 3d magnetic field alignment with vector vortex light, Phys. Rev. Lett. **127**, 233202 (2021).

[53] H. R. Hamedi, V. Kudriašov, J. Ruseckas, and G. Juzeliūnas, Azimuthal modulation of electromagnetically induced transparency using structured light, Opt. Express **26**, 28249 (2018).

[54] N. Radwell, T. W. Clark, B. Piccirillo, S. M. Barnett, and S. Franke-Arnold, Spatially dependent electromagnetically induced transparency, Phys. Rev. Lett. **114**, 123603 (2015).

[55] M. Abbas, U. Saleem, Rahmatullah, Y.-C. Zhang, and P. Zhang, Spontaneously generated structured light in a coherently driven five-level M-type atomic system, Phys. Rev. A **109**, 023716 (2024).

[56] S. H. Asadpour, M. Abbas, H. R. Hamedi, J. Ruseckas, E. Paspalakis, and R. Asgari, Spatiospectral control of spontaneous emission, Phys. Rev. A **110**, 033706 (2024).

[57] Y. Tang and A. E. Cohen, Optical chirality and its interaction with matter, Phys. Rev. Lett. **104**, 163901 (2010).

[58] S. Zhang, W. Ni, X. Kou, M. H. Yeung, L. Sun, J. Wang, and C. Yan, Formation of gold and silver nanoparticle arrays and thin shells on mesostructured silica nanofibers, Adv. Funct. Mater. **17**, 3258 (2007).

[59] J. Liu, H. Dong, Y. Li, P. Zhan, M. Zhu, and Z. Wang, A facile route to synthesis of ordered arrays of metal nanoshells with a controllable morphology, Jpn. J. Appl. Phys. **45**, L582 (2006).

[60] A. Modinos, V. Yannopapas, and N. Stefanou, Scattering of electromagnetic waves by nearly periodic structures, Phys. Rev. B **61**, 8099 (2000).

[61] V. Yannopapas and N. V. Vitanov, Electromagnetic green's tensor and local density of states calculations for collections of spherical scatterers, Phys. Rev. B **75**, 115124 (2007).

[62] V. Yannopapas, E. Paspalakis, and N. V. Vitanov, Plasmon-induced enhancement of quantum interference near metallic nanostructures, Phys. Rev. Lett. **103**, 063602 (2009).

[63] N. Stefanou, V. Yannopapas, and A. Modinos, A new version of the program for transmission and band-structure calculations of photonic crystals, Comput. Phys. Commun. **132**, 189 (2000).